Phase Separation from Electron Confinement at Oxide Interfaces

N. Scopigno,[1] D. Bucheli,[1] S. Caprara,[1,2] J. Biscaras,[3] N. Bergeal,[3] J. Lesueur,[3] and M. Grilli[1,2]
[1]*Dipartimento di Fisica, Università di Roma "Sapienza", Piazzale Aldo Moro 5, 00185 Roma, Italy*
[2]*ISC-CNR and Consorzio Nazionale Interuniversitario per le Scienze Fisiche della Materia, Unità di Roma "Sapienza"*
[3]*Laboratoire de Physique et d'Étude des Matériaux, CNRS-ESPCI ParisTech-UPMC, PSL Research University, 10 Rue Vauquelin, 75005 Paris, France*

(Received 25 June 2015; revised manuscript received 2 October 2015; published 15 January 2016)

Oxide heterostructures are of great interest for both fundamental and applicative reasons. In particular, the two-dimensional electron gas at the $LaAlO_3/SrTiO_3$ or $LaTiO_3/SrTiO_3$ interfaces displays many different properties and functionalities. However, there are clear experimental indications that the interface electronic state is strongly inhomogeneous and therefore it is crucial to investigate possible intrinsic mechanisms underlying this inhomogeneity. Here, the electrostatic potential confining the electron gas at the interface is calculated self-consistently, finding that such confinement may induce phase separation, to avoid a thermodynamically unstable state with a negative compressibility. This provides a robust mechanism for the inhomogeneous character of these interfaces.

DOI: 10.1103/PhysRevLett.116.026804

The two-dimensional electron gas (2DEG) that forms at the interface of two insulating oxides, like $LaAlO_3/SrTiO_3$ and $LaTiO_3/SrTiO_3$ (hereafter generically referred to as LXO/STO) [1–4], exhibits a rich phenomenology, such as a gate-tunable metal-to-superconductor transition [5–9], a magnetic-field-tuned quantum criticality [10], and inhomogeneous magnetic responses [11–16]. Tunneling [17,18], atomic force microscopy [19], SQUID magnetometry [20], and critical current [21] experiments provide clear evidence of an inhomogeneous interface on micro- and/or nanoscopic scales. Transport measurements report further signs of inhomogeneity and a percolative metal-to-superconductor transition with a sizable fraction of the 2DEG never becoming superconducting down to the lowest accessible temperatures [22–25]. For both fundamental reasons and applicative purposes, like design and control of the inhomogeneities and their patterning at the nano- or mesoscales, it is crucial to identify possible *intrinsic* mechanisms that may render the 2DEG so strongly inhomogeneous via a phase separation (PS). This is precisely the focus of the present work.

Here, we identify a very effective electron-driven mechanism leading to PS, based on the confinement of the 2DEG at the interface. From customary self-consistent calculations of the confining potential well in semiconductors, it is well known [26] that a finite lateral extension usually renders the 2DEG more compressible than its strictly 2D counterpart. This effect is much stronger in LXO/STO than in ordinary semiconductor interfaces, due to the huge dielectric constant of STO, allowing for much larger electron densities, with a strong amplification of the self-consistent adjustments of the confining potential. As a consequence, a nonrigid band structure arises, which varies with the local electron density: an increased electron density is accompanied by a corresponding increase of the positive countercharges (due to oxygen vacancies and/or polarity catastrophe [27–32]), from which the interfacial electrons are introduced and restoring the overall charge neutrality. For small-to-moderate increases of electron and countercharge densities the potential well deepens and the electron energy levels are shifted downwards. In this Letter we show that this mechanism leads *by itself* to PS.

The model.—The thermodynamic stability of the system is investigated by varying the density of the interfacial gas while keeping the overall neutrality. Therefore, a corresponding amount of positive countercharges has to be varied (see Fig. 1). Because of this tight connection between positive and negative charges the (in)stability will be determined by calculating the chemical potential of the whole system (i.e., of both the mobile electrons and of the other charges). While we will solve the quantum problem of the mobile electrons in the self-consistent confining well, the countercharges, the fraction of electrons trapped in impurity states of the bulk (see below), and the boundary conditions fixing the gating potential will determine the classical electrostatic energy of the system. All these contributions (for a detailed description see Ref. [33]) yield the total energy $\mathcal{E}$ and, in turn, the chemical potential $\mu = E(N+1) - E(N) \approx \partial_N E$ (here N represents the number of electrons, which is always kept equal to the number of countercharges).

The energy of the 2DEG is obtained through the calculation of the energy spectra as a function of the electron density, $n \equiv \delta n + n_0$ [henceforth, carrier densities, e.g., n, carrying no z dependence are meant per interfacial unit cell (u.c.), and are related to their z-dependent counterparts by relations like, e.g., $n = \int_0^\infty dz n(z)$]. Here, δn is the

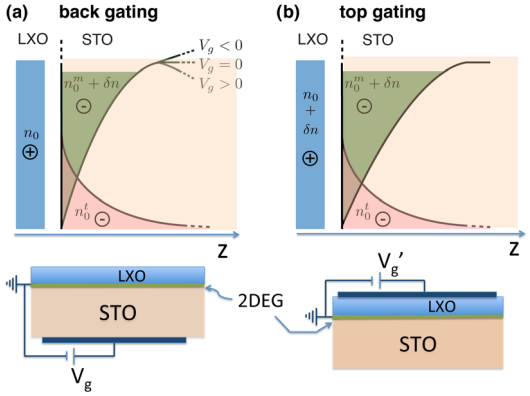

FIG. 1. Sketch of the interface for back (a) and top (b) gating. The upper part sketches the confining potentials, while the bottom part reports the structure of samples and electrodes. The confining potential depends on both mobile (n_0^m) and trapped (n_0^t) charges, which together compensate the positive countercharges n_0 in the LXO side. Applying a positive (negative) voltage V_g (or $V_g' \ll V_g$, in the case of topgating), δn electrons per unit cell are added to (subtracted from) the interface and the potential changes accordingly.

extrinsic component introduced by gating, while the intrinsic component n_0 [38] originates from the electronic reconstruction due to the polarity catastrophe and/or from oxygen vacancies within the LXO layer. Which of the two dominates is immaterial in our calculations and we represent the related positive countercharges as the light-blue shaded areas in the LXO side of Fig. 1.

What matters, instead, is the way the extrinsic charges are introduced, particularly in the case of backgating [Fig. 1(a)]: Applying a positive voltage V_g, the electrostatic potential, after increasing in the region close to the interface, decreases linearly with distance, once the interfacial charge density has been exhausted [the electrons reside on the STO side, assumed to occupy the $z > 0$ half space, and $n(z) \to 0$ for large z]. Then the electrons closest to the top of the well are weakly confined and some of them may escape and get trapped into the defects of bulk STO, as it is demonstrated by irreversibility effects under large backgating potentials [39]. Thus, in the absence of trapped charges, the quantum well is intrinsically unstable upon positive backgating. In the topgating configuration [Fig. 1(b)], the leakage also occurs, because the Fermi energy of the electrons, attracted to the interface by the positive V_g, exceeds the confining potential on the STO side. In both configurations, we are therefore led to introduce trapped charges that we describe by a distribution $n_0^t(z) = (n_0^t/\lambda)e^{-z/\lambda}$ on the STO side, decaying over a distance λ of several tens of nanometers (see pink shaded area in Fig. 1). This has the main effect of deepening the confining potential well, the Fermi energy being located substantially below its top (see, e.g., Refs. [8,40]).

The mobile electrons occupy energy levels that are quantized in the z direction and form a 2D band structure in the xy (interfacial) plane. The electrostatic potential $\phi(z)$ confining the electrons is determined self-consistently with the mobile electron density distribution $n^m(z) \equiv n_0^m(z) + \delta n(z)$ (at external gating V_g), for a frozen distribution of trapped charges $n_0^t(z)$. The z component of the factorized wave function $\Psi(x,y,z) = \zeta_{i\alpha}(z)\psi_{k_x k_y}(x,y)$ is the solution of the Schrödinger equation yielding the subband energy $\varepsilon_{i\alpha}$,

$$\left[\frac{\hbar^2}{2m_\alpha^z}\frac{d^2}{dz^2} + e\phi(z) + \varepsilon_{i\alpha}\right]\zeta_{i\alpha}(z) = 0, \tag{1}$$

where the electron charge is $-e$, $i = 1, 2, 3, \ldots$ is the subband index, and $\alpha = xy, xz, yz$ labels the Ti t_{2g} orbitals, d_{xy}, d_{xz}, d_{yz}, where the electrons mostly reside. While the details of the band structure are reported in Ref. [33], according to standard values [41], we take $m_l = 0.7m_e$ and $m_h = 14m_e$ (m_e is the electron mass).

Assuming full translational invariance along the xy planes and integrating over a u.c. of area a^2, the density of mobile electrons, at temperature $T = 0$, reads

$$n^m(z) = \sum_{i\alpha} |\zeta_{i\alpha}(z)|^2 \int_{-\infty}^{\varepsilon_F} d\varepsilon g_{i\alpha}(\varepsilon),$$

where $g_{i\alpha}(\varepsilon) = a^2(\pi\hbar^2)^{-1}\sqrt{m_\alpha^x m_\alpha^y}\,\theta(\varepsilon - \varepsilon_{i\alpha})$ is the density of states (DOS) of the various t_{2g} subbands, $\theta(\varepsilon)$ is the Heaviside function, and ε_F is the Fermi energy.

The electron distribution corresponds to an electrostatic potential $\tilde{\phi}(z)$ obeying the Poisson equation:

$$\frac{\epsilon_0 a^2}{e}\frac{d}{dz}\left[\epsilon_r(E)\frac{d}{dz}\tilde{\phi}(z)\right] = n^m(z) + n_0^t(z). \tag{2}$$

Here, the dielectric constant is a function of the electric field $E = -d\tilde{\phi}/dz$ via the relation $\epsilon_r(E) = (A + B|E|)^{-1} + \epsilon_\infty$, where A, B, and ϵ_∞ are experimentally measured constants [42]. Owing to the nearly ferroelectric character of STO, ϵ_r can reach very large values ($\gtrsim 25 \times 10^3$) but, due to the very strong interfacial electric field [8,43,44], we find that, near $z = 0$, $\epsilon_r \approx \epsilon_\infty \approx 100$–$300$. The point of the above derivation is that the calculation is self-consistent only if the two potentials, ϕ from Eq. (1) and $\tilde{\phi}$ from Eq. (2), coincide.

Besides the difficulties stemming from the self-consistency, there are additional subtleties coming from the boundary conditions, which vary for the back- or topgating configuration. In the former case we fix a density of positive charges $n_0 = \int_0^\infty dz[n_0^m(z) + n_0^t(z)]$ at $z = 0^-$. This simplifying choice, which turns out to be slightly less favorable to the occurrence of PS, avoids the distinction between the case of oxygen vacancies (for which the countercharges would be uniformly distributed in the LXO) and the polarity catastrophe (in which the countercharges suitably distribute themselves in the polar planes of LXO in order to minimize the energy [45]). Having fixed the positive charges, we consider the electric field at $z = 0^+$

(i.e., the slope of the confining potential) at the interface. The electric field deep inside the STO [where $n_0(z) \to 0$] is fully determined by the gate potential because the intrinsic electronic density and the corresponding positive charges in the LXO compensate and have thus no effect in this region [see Fig. 1(a)]. On the other hand, the electrons coming from backgating create a field V_g/L, with $e\delta n = \epsilon_0 a^2 \int_0^{V_g/L} \epsilon_r(E) dE$, where L is the thickness of the STO substrate. In the topgating configuration, instead, the density of positive charges at $z = 0^-$ amounts to $n_0 + \delta n$, and the electric field vanishes deep inside the STO substrate [see Fig. 1(b)].

Once the quantum problem of mobile electrons is solved, the rest of the energy is due to the electrostatic contribution (per u.c.) of electric fields due to the overall distribution of the mobile (m) and the fixed (f, from gates and trapped) charges

$$\mathcal{E}_{es} = \frac{\epsilon_0 a^2}{2} \int_{-\infty}^{\infty} \epsilon_r(E)[E^{f2}(z) - E^{m2}(z)]dz, \qquad (3)$$

with $E = E^f + E^m$. Notice that, since the Hartree-like electrostatic energy is double-counted in the quantum Hamiltonian, the contribution of the mobile charges must be subtracted in Eq. (3). In Ref. [33] we provide details of how the above fields are calculated.

Results.—To show that the electron confinement is the driving mechanism of PS we first consider the pure quantum problem neglecting the classical electrostatic contributions to the free energy. We thus report in Fig 2(a) the evolution of the different subband levels as a function of the mobile electron density n^m, which is the sum of the as grown carrier density n_0^m and the extra charges δn added by electrostatic gating. This evolution is a direct consequence of the nonrigidity of the bands. The resulting Fermi energy ε_F is goes up as expected, while the chemical potential μ^m of the mobile electrons has nonmonotonic behavior. Indeed, when ε_F crosses the first heavy band ($d_{xz,yz}$ which have the largest DOS along the xy plane), μ^m starts to decrease. The most important result of this Letter is that, for a given range of mobile electron densities, the chemical potential decreases while electrons are added, resulting in a region of negative compressibility in the phase diagram. This region is delimited by a spinodal line where the compressibility diverges (i.e., μ has a maximum or a minimum as a function of the density). To identify the region where the homogeneous system is thermodynamically stable one has to perform a standard Maxwell construction. The Maxwell construction region encloses the spinodal region and it identifies the region where the thermodynamic instability is prevented by PS, with the consequent inhomogeneous redistribution of electrons and countercharges. Our calculations lead to the chemical potential displayed in the panels of Figs. 2(b)–2(d) (orange dashed lines) when n^m is increased (the gate voltage is kept constant in this calculation, while n_0^m is varied).

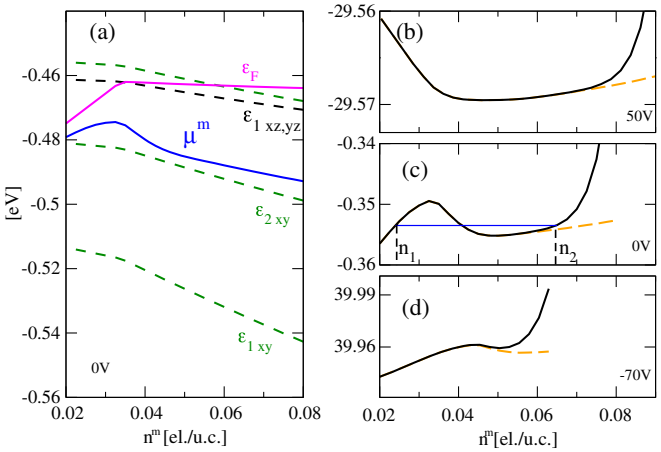

FIG. 2. (a) Fermi energy (magenta solid line), electron-only (see text) chemical potential (blue solid line), subband levels (green dashed for the d_{xy} and black dashed for the $d_{xz,yz}$ levels) as a function of the build-in density n_0 at zero gating potential. (b) Chemical potential as a function of the mobile electron density $n^m = n_0^m + \delta n$ at fixed values of the backgating potential $V_g(\delta n)$ (the δn electrons due to gating are thus also fixed). The orange dashed (black solid) lines correspond to the solution in the absence (presence) of a short-range background contribution to the chemical potential of the form $\mu_{sr}(n^m) = A[(n^m - \delta n)/0.065]^p$, where the exponent $p = 19$ measures the short-range rigidity and $A = 7 \times 10^{-4}$ eV. For $V_g = 50$ V, $\delta n = 0.0137$. (c) Same as (b) with $\delta n = 0$. The thin solid blue line provides an example of Maxwell construction. The densities n_1 and n_2 delimit the miscibility gap. (d) Same as (b) with $\delta n = -0.0171$.

The Maxwell construction results in a very broad PS region delimited by the dashed orange lines in the phase diagrams of Fig 3(a) and 3(b) for back- and topgating, respectively. As it can be seen, the miscibility gap extends on a very broad range of densities and voltages. This raises the issue of mechanisms which are present in the real systems to limit this otherwise strong PS tendency. A microscopic modeling of such interactions is exceedingly difficult, but they can be considered within a phenomenological scheme. For instance, while we already took into account the long-range electrostatic cost of the charge distribution, we did not include in our model any short range repulsion between the countercharges (oxygen vacancies or positive charges left by the polarity catastrophe reconstruction). While some mild fluctuations of electrons and compensating countercharges are acceptable, when too many electrons segregate carrying along too large densities of countercharges, the system becomes very rigid and the charge segregation stops. To phenomenologically describe this physics, we added a short-range repulsion to the total energy, that induces a rapid growth in $\mu(n)$ when electron densities above those experimentally found (with a maximum of 0.5 el/u.c., including the trapped charges) are reached. Because of this additional short-range mechanism, the PS region determined by the Maxwell construction on

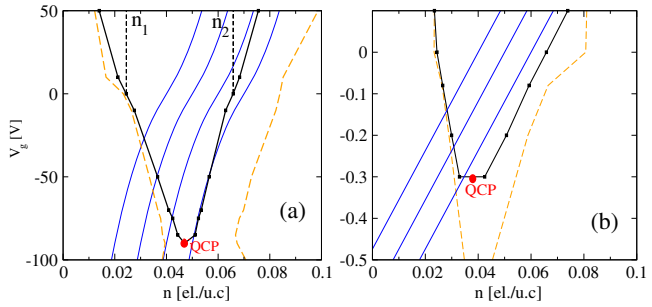

FIG. 3. (a) Gate potential versus mobile electron density phase diagram for the backgated LXO/STO interface in the absence (orange dashed lines) and in the presence (black solid lines) of short-range rigidity of the countercharges. n_1 and n_2 are determined by the Maxwell construction exemplified in Fig. 2(c). The blue thin solid lines correspond to $n_0 = 0.04,\ 0.05,\ 0.06,\ 0.07$ el/u.c. at $V_g = 0$. (b) Same as (a) for the topgating case, with $n_0 = 0.04,\ 0.05,\ 0.06$ el/u.c. Notice that, despite the different voltage scale, due to the different ϵ_r and thickness of LXO and STO, the electron densities and confining electric fields are comparable.

the black solid lines of Figs. 2(b)–2(d) is reduced [black solid lines and squares in Figs. 3(a) and 3(b)] and, quite remarkably, it ends with a critical point at some critical negative gate value, V_g^c.

The initial (as-grown) density n_0 is determined by several factors (like, e.g., the number of LXO planes). Starting from a given n_0, the total density, $n = n_0 + \delta n$, is then changed by the gating following the thin blue trajectories in the phase diagram. Upon decreasing the gating the overall average density n decreases and the fraction of the system with lower density n_1 increases, in agreement with transport measurements [24,25,46], until the system exits the PS region at some negative voltage.

Discussion.—From Figs. 3(a) and 3(b) one can see that there exists a broad range of the intrinsic density n_0 yielding a negative compressibility, prevented by PS. This PS yields an inhomogeneous 2DEG with associated inhomogeneity of the oxygen vacancies and/or electronic reconstructions. We carried out a detailed analysis (see also Ref. [33]) to identify the specific mechanisms determining this instability finding that it arises from two main features peculiar to these oxide interfaces.

First of all, a larger n_0 corresponds to larger countercharge density on the LXO side, which attracts the interface electrons and deepens the confining potential well, causing a downward shift of the quantized levels. Second, the electrons at the interface are confined on the STO side, where a large dielectric constant $(\epsilon_r > \epsilon_\infty \gtrsim 100)$ efficiently screens the electric fields. This allows for a large electron density ($\approx 10^{13}$ cm^{-2}), with the electrons residing on several confined subbands. The large DOS coming from the contributions of the individual subbands enhances the electron compressibility, facilitating the instability. This effect is stronger when $d_{xz,yz}$ subbands, with larger DOS, start to be filled. The relevance of the $d_{xz,yz}$ levels has already been asserted in Hartree-Fock calculations [47] and seems to be experimentally supported [48]. The filling of these levels typically starts when the system enters the PS dome upon increasing V_g, and rapidly leads to increasingly more abundant regions with locally higher electron density. We speculate that this corresponds to the observed increase of high-mobility carriers [8,24]. If one is willing to accept the idea that only regions with higher electron densities can become superconducting, the increasingly large number of these regions can account for the occurrence of an inhomogeneous superconducting state above some (percolative) threshold [22–25,46].

Interestingly, in a rather large range of n_0 values, the system exits the PS dome in the vicinity of the quantum critical point (QCP) located at $n_0^c \approx 0.0475$ el/u.c. and $V_g^c \approx -90$ V for backgating (see blue line trajectories in Fig. 3). These values are well within the range experimentally found for the gate potentials of the superconducting onsets [6,8,49], indicating that the real systems exit the PS dome not far from the QCP. This also suggests that decreasing V_g, the electrons in the LXO/STO interface should eventually display some signatures of critical behavior where superconductivity will likely be affected by the strong quantum density fluctuations [49,50].

In conclusion, we identified a mechanism of electron-driven PS. While the details of the phase-separated region also depend on the short-range rigidity of the system, the existence and robustness of the PS is a generic result and can be responsible for the strong inhomogeneity observed at LXO/STO interfaces. This mechanism can also cooperate with extrinsic defects (e.g., domain walls [20,51]) or with other intrinsic mechanisms based on short range interactions, like the Rashba spin-orbit coupling [43,44] or the local electronic effects of oxygen vacancies [52], which are specific of the LXO/STO systems. On the other hand, owing to the rather generic character of the mechanism considered here, our work might also be relevant for other surface or interface states, like, e.g., in topologic insulators, where inhomogeneities turn out to be quite common.

We thank V. Brosco, C. Castellani, R. Raimondi, and G. Seibold for stimulating discussions. We acknowledge financial support from the Sapienza University Project No. C26A115HTN, the CNRS PICS program "S2S," the ANR JCJC "Nano-SO2DEG," the SESAME, OXYMORE, and CNano programs from Région IdF.

[1] A. Ohtomo and H. Y. Hwang, Nature (London) **427**, 423 (2004).
[2] J. Mannhart, D. H. A. Blank, H. Y. Hwang, A. J. Millis, and J. M. Triscone, MRS Bull. **33**, 1027 (2008).
[3] J. Mannhart and D. G. Schlom, Science **327**, 1607 (2010).
[4] H. Y. Hwang, Y. Iwasa, M. Kawasaki, B. Keimer, N. Nagaosa, and Y. Tokura, Nat. Mater. **11**, 103 (2012).

[5] N. Reyren *et al.*, Science **317**, 1196 (2007).
[6] A. D. Caviglia, S. Gariglio, N. Reyren, D. Jaccard, T. Schneider, M. Gabay, S. Thiel, G. Hammerl, J. Mannhart, and J.-M. Triscone, Nature (London) **456**, 624 (2008).
[7] J. Biscaras, N. Bergeal, A. Kushwaha, T. Wolf, A. Rastogi, R. C. Budhani, and J. Lesueur, Nat. Commun. **1**, 89 (2010).
[8] J. Biscaras, N. Bergeal, S. Hurand, C. Grossetête, A. Rastogi, R. C. Budhani, D. LeBoeuf, C. Proust, and J. Lesueur, Phys. Rev. Lett. **108**, 247004 (2012).
[9] S. Hurand *et al.*, Sci. Rep. **5**, 12751 (2015).
[10] J. Biscaras, N. Bergeal, S. Hurand, C. Feuillet-Palma, A. Rastogi, R. C. Budhani, M. Grilli, S. Caprara, and J. Lesueur, Nat. Mater. **12**, 542 (2013).
[11] Ariando *et al.*, Nat. Commun. **2**, 188 (2011).
[12] L. Li, C. Richter, J. Mannhart, and R. C. Ashoori, Nat. Phys. **7**, 762 (2011).
[13] J. A. Bert, B. Kalisky, C. Bell, M. Kim, Y. Hikita, H. Y. Hwang, and K. A. Moler, Nat. Phys. **7**, 767 (2011).
[14] D. A. Dikin, M. Mehta, C. W. Bark, C. M. Folkman, C. B. Eom, and V. Chandrasekhar, Phys. Rev. Lett. **107**, 056802 (2011).
[15] M. M. Mehta, D. A. Dikin, C. W. Bark, S. Ryu, C. M. Folkman, C. B. Eom, and V. Chandrasekhar, Nat. Commun. **3**, 955 (2012).
[16] J. A. Bert *et al.*, Phys. Rev. B **86**, 060503(R) (2012).
[17] C. Richter *et al.*, Nature (London) **502**, 528 (2013).
[18] D. Bucheli, S. Caprara, and M. Grilli, Supercond. Sci. Technol. **28**, 045004 (2015).
[19] F. Bi, M. Huang, C. Wung Bark, S. Ryu, S. Lee, C.-B. Eom, P. Irvin, and J. Levy, arXiv:1302.0204.
[20] B. Kalisky *et al.*, Nat. Mater. **12**, 1091 (2013).
[21] G. E. D. K. Prawiroatmodjo, F. Trier, D. V. Christensen, Y. Chen, N. Pryds, and T. S. Jespersen, arXiv:1510.01199.
[22] S. Caprara, M. Grilli, L. Benfatto, and C. Castellani, Phys. Rev. B **84**, 014514 (2011).
[23] D. Bucheli, S. Caprara, C. Castellani, and M. Grilli, New J. Phys. **15**, 023014 (2013).
[24] S. Caprara, J. Biscaras, N. Bergeal, D. Bucheli, S. Hurand, C. Feuillet-Palma, A. Rastogi, R. C. Budhani, J. Lesueur, and M. Grilli, Phys. Rev. B **88**, 020504(R) (2013).
[25] S. Caprara *et al.*, SPIN **04**, 1440004 (2014).
[26] J. P. Eisenstein, L. N. Pfeiffer, and K. W. West, Phys. Rev. B **50**, 1760 (1994).
[27] The origin of the interfacial electrons is still controversial. Besides the electronic reconstruction mechanism related to the polarity catastrophe [28], the occurrence of oxygen vacancies is widely considered and controversial [29–31]. See also Ref. [32], and references therein.
[28] N. Nakagawa, H. Y. Hwang, and D. A. Muller, Nat. Mater. **5**, 204 (2006).
[29] Y. Chen, N. Pryds, J. E. Kleibeuker, G. Koster, J. Sun, E. Stamate, B. Shen, G. Rijnders, and S. Linderoth, Nano Lett. **11**, 3774 (2011).
[30] G. De Luca, A. Rubano, E. di Gennaro, A. Khare, F. M. Granozio, U. S. di Uccio, L. Marrucci, and D. Paparo, Appl. Phys. Lett. **104**, 261603 (2014).
[31] E. Di Gennaro, U. Coscia, G. Ambrosone, A. Khare, F. M. Granozio, and U. S. di Uccio, Sci. Rep. **5**, 8393 (2015).
[32] L. Yu and A. Zunger, Nat. Commun. **5**, 5118 (2014).
[33] See Supplemental Material at http://link.aps.org/supplemental/10.1103/PhysRevLett.116.026804 for a detailed description of the iterative procedure, for the numerical solution of the Schrödinger and Poisson equations, and for the calculation of the electrostatic contribution to the total energy. The Supplemental Material includes Refs. [34–37].
[34] F. Stern and W. E. Howard, Phys. Rev. **163**, 816 (1967).
[35] M. Salluzzo *et al.*, Phys. Rev. Lett. **102**, 166804 (2009).
[36] Z. Zhong, A. Tóth, and K. Held, Phys. Rev. B **87**, 161102 (R) (2013).
[37] L. R. Ram-Mohan, *Finite Element and Boundary Element Applications in Quantum Mechanics* (Oxford University Press, New York, 2002).
[38] The gate potential V_g (and the associated density δn) are external parameters determining the thermodynamic state of the system. In contrast, the density n_0 and its fluctuations are determined by the internal stability of the system. Thus, establishing whether for a given value of n_0, say n_0^{exp} (fixed by the chemistry of the sample), the 2DEG is stable or not, amounts to determine whether the chemical potential is an increasing or a decreasing function of n_0 in the vicinity of n_0^{exp}, while keeping $V_g \propto \delta n$ fixed.
[39] J. Biscaras, S. Hurand, C. Feuillet-Palma, A. Rastogi, R. C. Budhani, N. Reyren, E. Lesne, J. Lesueur, and N. Bergeal, Sci. Rep. **4**, 6788 (2014).
[40] W. Meevasana, P. D. C. King, R. H. He, S-K. Mo, M. Hashimoto, A. Tamai, P. Songsiriritthigul, F. Baumberger, and Z-X. Shen, Nat. Mater. **10**, 114 (2011).
[41] A. F. Santander-Syro *et al.*, Nature (London) **469**, 189 (2011).
[42] R. Neville, C. Mead, and B. Hoeneise, J. Appl. Phys. **43**, 2124 (1972).
[43] S. Caprara, F. Peronaci, and M. Grilli, Phys. Rev. Lett. **109**, 196401 (2012).
[44] D. Bucheli, M. Grilli, F. Peronaci, G. Seibold, and S. Caprara, Phys. Rev. B **89**, 195448 (2014).
[45] K. Steffen, F. Loder, and T. Kopp, Phys. Rev. B **91**, 075415 (2015).
[46] S. Caprara, D. Bucheli, N. Scopigno, N. Bergeal, J. Biscaras, S. Hurand, J. Lesueur, and M. Grilli, Supercond. Sci. Technol. **28**, 014002 (2015).
[47] Se Y. Park and A. J. Millis, Phys. Rev. B **87**, 205145 (2013).
[48] A. Joshua, S. Pecker, J. Ruhman, E. Altman, and S. Ilani, Nat. Commun. **3**, 1129 (2012).
[49] S. Hurand, J. Biscaras, N. Bergeal, C. Feuillet-Palma, G. Singh, A. Jouan, A. Rastogi, A. Dogra, R. C. Budhani, S. Caprara, M. Grilli, and J. Lesueur, arxiv:1506.06874.
[50] S. Caprara, N. Bergeal, J. Lesueur, and M. Grilli, J. Phys. Condens. Matter **27**, 425701 (2015).
[51] N. C. Bristowe, T. Fix, M. G. Blamire, P. B. Littlewood, and E. Artacho, Phys. Rev. Lett. **108**, 166802 (2012).
[52] N. Pavlenko, T. Kopp, and J. Mannhart, Phys. Rev. B **88**, 201104(R) (2013).